eNeuro

Research Article: New Research | Integrative Systems

Development of a mouse reporter strain for the purinergic $P2X_2$ receptor

https://doi.org/10.1523/ENEURO.0203-20.2020

Cite as: eNeuro 2020; 10.1523/ENEURO.0203-20.2020

Received: 19 May 2020
Revised: 23 June 2020
Accepted: 3 July 2020

Title: Development of a mouse reporter strain for the purinergic $P2X_2$ receptor

Abbreviated title: $P2X_2$ reporter mouse

Seol-Hee Kim, Parmvir K Bahia, Mayur Patil, Sydney Sutton, Isobel Sowells, Stephen H Hadley, Marian Kollarik, Thomas E Taylor-Clark*

Molecular Pharmacology & Physiology, Morsani College of Medicine, University of South Florida, Tampa, FL 33612, USA.

* Corresponding author: Thomas E Taylor-Clark, 12901 Bruce B Downs Blvd, Tampa, FL 33612, USA. ttaylorclark@usf.edu

Number of Figures: 9
Number of words abstract: 246
Number of words introduction: 654
Number of words discussion: 2213

Acknowledgements: This work was supported by the National Institutes of Health's Office of Director SPARC Commonfund program (OT2OD023854), the National Institute for Neurological Disorders and Stroke (U01NS113868) and the National Institute of Diabetes and Digestive and Kidney Diseases (R01DK110366 and U01DK116311).

Conflicts of Interest: The authors declare no competing financial interests.

Abstract

The ATP-sensitive $P2X_2$ ionotropic receptor plays a critical role in a number of signal processes including taste and hearing, carotid body detection of hypoxia, the exercise pressor reflex and sensory transduction of mechanical stimuli in the airways and bladder. Elucidation of the role of $P2X_2$ has been hindered by the lack of selective tools. In particular, detection of $P2X_2$ using established pharmacological and biochemical techniques yields dramatically different expression patterns, particularly in the peripheral and central nervous systems. Here, we have developed a knockin $P2X_2$-cre mouse, which we crossed with a cre-sensitive tdTomato reporter mouse to determine $P2X_2$ expression. $P2X_2$ was found in more than 80% of nodose vagal afferent neurons, but not in jugular vagal afferent neurons. Reporter expression correlated in vagal neurons with sensitivity to $\alpha\beta$mATP. $P2X_2$ was expressed in 75% of petrosal afferents, but only 12% and 4% of dorsal root ganglia and trigeminal afferents, respectively. $P2X_2$ expression was limited to very few cell types systemically. Together with the central terminals of $P2X_2$-expressing afferents, reporter expression in the CNS was mainly found in brainstem neurons projecting mossy fibers to the cerebellum, with little expression in the hippocampus or cortex. The structure of peripheral terminals of $P2X_2$-expressing afferents was demonstrated in the tongue (taste buds), carotid body, trachea and esophagus. $P2X_2$ was observed in hair cells and support cells in the cochlear, but not in spiral afferent neurons. This mouse strain provides a novel approach to the identification and manipulation of $P2X_2$-expressing cell types.

Significance statement

Inhibitor and knockout studies have demonstrated the critical role of $P2X_2$ in multiple sensory signaling pathways. Nevertheless, $P2X_2$ expression patterns are controversial, as biochemical studies suggest widespread expression whereas functional studies suggest restricted expression. Functional characterization is further complicated by heteromeric $P2X_{2/3}$ channels that have hybrid pharmacology and biophysical properties. We have developed a $P2X_2$-cre mouse to determine the expression pattern of $P2X_2$. In the periphery, $P2X_2$ expression is found in almost all nodose sensory afferents but is limited to only minor subsets of trigeminal and DRG afferents. Centrally, $P2X_2$ is mostly expressed in neurons projecting mossy fibers to the cerebellum. Thus we provide novel evidence for the specific expression of $P2X_2$, which is more limited than previously thought.

Introduction

$P2X_2$ is one of seven members of the P2X purinergic receptor family (Brake et al., 1994; Dunn et al., 2001; Khakh et al., 2001). $P2X_2$ is a cation-permeable plasma membrane ion channel activated by extracellular ATP, which can form either functional homomeric channels or functional heteromeric channels with $P2X_3$ (Brake et al., 1994; Chen et al., 1995; Lewis et al., 1995). Based upon pharmacological and genetic knockout studies, $P2X_2$ plays important roles in a number of peripheral organs, including taste cell signaling to gustatory sensory afferents (Finger et al., 2005; Huang et al., 2011), hypoxic signaling in carotid bodies (Rong et al., 2003), protection from noise-induced ototoxicity (Yan et al., 2013), the exercise pressor reflex (McCord et al., 2010) and mechanical transduction in sensory afferents innervating the airways (Weigand et al., 2012) and bladder (Cockayne et al., 2005). Nevertheless, the precise role of $P2X_2$ in peripheral afferents and in other systems is hindered by the lack of selective tools.

$P2X_2$ and $P2X_3$ homomeric channels can be discriminated by the desensitization of their ATP-evoked currents (limited desensitization/persistent currents for $P2X_2$ channels, rapid desensitization for $P2X_3$) and their sensitivity to α,β methylene ATP ($\alpha\beta$mATP, $P2X_3$ is activated by this ATP analog, whereas $P2X_2$ is not) (Dunn et al., 2001; Khakh et al., 2001). Nevertheless, co-expression of $P2X_2$ and $P2X_3$ causes the formation of heteromeric $P2X_{2/3}$ channels that evoke mixed/persistent currents in response to both ATP and $\alpha\beta$mATP (Lewis et al., 1995). Furthermore, the kinetics of P2X channel desensitization are modulated by numerous factors (Bianchi et al., 1999; Sokolova et al., 2006), thus decreasing its effectiveness as a diagnostic for discriminating $P2X_2$, $P2X_3$ and $P2X_{2/3}$ channels. Biochemical detection of $P2X_2$ reveals similar inconsistencies: immunohistochemistry and in situ hybridization has revealed robust and widespread expression of $P2X_2$ in peripheral and central neurons and smooth muscle (Brake et al., 1994; Kidd et al., 1995; Collo et al., 1996; Vulchanova et al., 1996; Kanjhan et al., 1999; Petruska et al., 2000b; Yao et al., 2000; Gourine et al., 2003; Yao et al., 2003; Spehr et al., 2004; Ambalavanar et al., 2005; Cockayne et al., 2005; Simonetti et al., 2006; Staikopoulos et al., 2007; Song et al., 2012), although functional studies of ATP- and $\alpha\beta$mATP-evoked currents suggest a much more limited expression pattern. As such there is considerable uncertainty regarding the expression of $P2X_2$, despite its established role in cellular signaling, particularly in the peripheral nervous system (Rong et al., 2003; Cockayne et al., 2005; Finger et al., 2005; McCord et al., 2010; Huang et al., 2011; Weigand et al., 2012).

Here, we used genetic targeting of the endogenous $P2X_2$ locus to generate a knockin reporter mouse that expresses Cre recombinase in $P2X_2$-expressing cells. After crossing this strain with a cre-sensitive tdTomato reporter mouse strain, we visualized $P2X_2$ expression in sensory ganglia, the CNS and in peripheral tissues. We found robust reporter expression in nodose vagal neurons but not in jugular vagal neurons, and reporter expression was limited to few neurons in the trigeminal ganglia and dorsal root ganglia (DRG). We confirmed the expression of $P2X_2$ in tdTomato-expressing vagal neurons by assessing Ca^{2+} influx in response to the $P2X_{2/3}$ agonist α,β methylene ATP ($\alpha\beta$mATP) using Fura 2AM. Reporter expression was used to visualize $P2X_2$-expressing terminals in the tongue, carotid body, trachea and esophagus as well as in the nucleus tractus solitarius (nTS) in the dorsal medulla (the location of central terminations of nodose sensory afferents). Elsewhere in the CNS, reporter expression was largely limited to medullary and pontine neurons protecting mossy fibers to the cerebellum, although reporter expression was also noted in a small number of cerebellar purkinje neurons, cerebral cortical neurons and caudoputamen neurons. Lastly, we observed expression in hair cells and support cells in the organ of Corti in the cochlea. Thus, this reporter mouse demonstrates the specific expression of the purinergic receptor $P2X_2$ and provides a novel tool to study the structure and function of these particular cells.

Methods

Knockin mouse model development

The gene for the murine $P2X_2$ receptor (P2rx2 gene, NCBI Reference Sequence: NM_153400.4) is located on chromosome 5. Eleven exons have been identified, with the ATG start codon in exon 1 and TGA stop codon in exon 11. In order to develop a knockin mouse that expresses Cre recombinase dependent on $P2X_2$ expression, the $P2X_2$ TGA stop codon was replaced with a 2A-Cre cassette (Fig. 1). The targeting vector homology arms were generated by high fidelity Taq PCR using BAC clone RP23-333M22 and RP23-354O18 from the C57BL/6J library as template. The targeting vector was assembled with recombination sites and selection markers: Neomycin resistance gene (Neo^R) flanked by self-deletion anchor (SDA) sites for positive selection and diphtheria toxin A fragment gene (DTA) for negative selection. Correct targeting vector synthesis was confirmed by appropriate digestion by restriction enzymes. The linearized vector was subsequently delivered to C57BL/6 ES cells via electroporation, followed by drug selection, PCR screening, and Southern Blot confirmation. After gaining 94 neomycin-

resistant clones, 18 potentially targeted clones were confirmed, 5 of which were expanded for Southern Blotting. After confirming correctly targeted ES clones via Southern Blotting, clones were selected for blastocyst microinjection, followed by founder production. Founders were confirmed as germline-transmitted via crossbreeding with wild-type. All aspects of knockin mouse development were performed by Cyagen US Inc (California). Founders were mated to produce heterozygous and homozygous mice ($P2rx2^{tm1.1(cre)Ttc}$, MGI:2665170) in expected Mendelian proportions. These mice express $P2X_2$-2A-Cre from the endogenous $P2X_2$ gene. Upon translation, the 2A peptide self-cleaves (Furler et al., 2001) to release $P2X_2$ and Cre as separate peptides. $P2rx2^{tm1.1(cre)Ttc}$ mice develop normally and were observed to have no apparent phenotype. Homozygous $P2rx2^{tm1.1(cre)Ttc}$ were crossed with the ROSA26-loxP-STOP-loxP-tdTomato mice (B6.Cg-Gt(ROSA)26Sortm9(CAG-tdTomato)Hze/J, #007909, Jackson Laboratory) to produce $P2X_2^{Cre/+}$/ROSA26-$tdTomato^{fl/+}$ ($P2X_2$-tdTomato mice), with cell-specific expression of tdTomato via Cre recombination. Specific alleles were confirmed by genotyping per developers' instructions. Both male and female mice (6 to 8-week-old) were used for experiments. Offspring were weaned at 21 postnatal days and up to 4 littermates were housed per cage under normal condition (20 ºC, a 12hrs dark/light cycle). Mice were provided with standard rodent chow and water *ad libitum*. All procedures were in accordance with the animal protocol approved by the Institutional Animal Care and Use Committee.

Tissue collection and immunofluorescence

Mice were euthanized by CO_2 inhalation and transcardially perfused with ice-cold PBS followed by perfusion fixation with ice-cold 3.7% formaldehyde (FA). Vagal ganglia, petrosal ganglia, trigeminal ganglia, thoracic dorsal root ganglia (DRG, T_1-T_5) and carotid body were dissected out and post-fixed for 1 hours in 3.7% FA at 4ºC. Medulla, spinal cord and tongue were collected and post-fixed for 4 hours in 3.7% FA at 4ºC. Brain were collected and post-fixed overnight in 3.7% FA at 4ºC. For the cochlea, the temporal bones were collected and post-fixed in 4% PFA overnight at 4ºC. The temporal bones were washed three times in PBS for 10 min and transferred to 10% ethylenediaminetetraacetic acid (EDTA, dissolved in H_2O, pH 7.2) solution for overnight decalcification at 4ºC. Tissue firmness was checked by pressing tissue with forceps to ensure adequate decalcification.

All tissues were washed in PBS to remove residual FA and transferred to 20% sucrose solution for cryoprotection. Tissue were mounted in OCT (optimal cutting temperature) compound and

snap frozen in dry ice prior to cryosectioning: sensory ganglia (20µm), carotid bodies (20µm), tongue (40µm), cochlea (40µm), spinal cord (20µm), medulla (40µm for coronal, 80µm for sagittal) and brain (80µm). All slices were collected onto Superfroast plus slides. Slides were then air-dried at room temperature in the dark overnight. For immunofluorescence, sectioned tissue was permeabilized with 0.3% Triton X-100 in PBS (PBSTx) for 15 min followed by blocking with 1% bovine serum albumin (BSA)/10% Donkey Serum (DS)/0.3% PBSTx. Sectioned tissue was incubated with primary antibodies diluted in blocking buffer overnight at 4 ºC. Sensory ganglia slices were stained for immunoreactivity to TRPV1 (Goat, 1:150, sc-12498, Santa Cruz), the neurotrophin receptors tyrosine receptor kinase A (TRKA) (Rabbit, 1:300, 06-574, Millipore) or pgp9.5 (Rabbit, 1:300, AB5925, Millipore). Carotid body slices were immunostained against tyrosine hydroxylase (TH) (Rabbit, 1:300, AB112, Abcam). Sequentially sectioned medulla slices were stained against TRPV1 (Guinea pig, 1:150, GP14100, Neuromics). After washing with 0.2% Tween 20 in PBS (PBST) three times for 10 min, tissue was incubated with appropriate secondary antibodies (chicken anti-goat 647 (1:300, A212345, Invitrogen), donkey anti-rabbit 488 (1:300, A21206, Invitrogen) and donkey anti-guinea pig 647 (1:300, AP193SA6, Millipore)) in 1% BSA/5% DS in 0.2% PBST for 1h. Tissue was washed with 0.2% PBST three times for 10 min and rinsed briefly with H_2O. In some cases, sectioned tissue was counter-stained with either green or blue fluorescent Nissl staining (1:600, NeuroTrace™ 500/525 or 435/455, Fluorescent Nissl Stain, Invitrogen). Slides were air-dried and mounted with DPX mounting medium (Sigma) or mounted with VECTASHIELD Antifade Medium with DAPI (Vector laboratories).

Whole-mount immunostaining of trachea and esophagus

The mouse trachea was split lengthwise by making a single cut through the midline. The esophagus was cut around the stomach and then split lengthwise. The mucosal and muscle layers of the esophagus were separated carefully by small sharp dissection scissors. We stained the trachea by first permeabilizing with 1% Tween 20 (Sigma-Aldrich, St. Louis, MO) in filtered 1X phosphate buffered saline (PBS) for 6 hours at room temperature, then washed three times for 20 minutes in filtered 1x PBS using rotator. Permeabilized tracheal tissues were incubated with rabbit anti-RFP primary antibody (1:200, 600-401-379, Rockland antibodies) in PBS with 1% BSA for 48 hours at 4°C (repositioned 5-6 times during incubation), washed in filtered 1x PBS ten times using rotator at 4°C, incubated with secondary antibody goat-anti-rabbit Alexa Fluor™ 568 (Molecular Probes) with dilution 1:100 in filtered 1x PBS for 5 hours at

room temperature. Trachea were then washed in filtered 1x PBS (three times, rotator, 4°C), incubated in anti-fade glycerol (pH=8.6, 10x Tris buffered-saline mixed with glycerol) for 24 hours at room temperature and stored in anti-fade glycerol at 4°C. The esophageal tissues went through the same treatment as the trachea, but the main difference was that we amplified the tdTomato signal by using a streptavidin-biotin protocol. In short, after the primary antibody step the tissues were washed in 1X PBS and then incubated with goat biotin-XX conjugate anti-rabbit IgG (H+L) secondary antibody (1:100, B2770, Molecular Probes) in 1% PBS/BSA overnight at room temperature (repositioned 1-2 times during incubation), washed in filtered 1x PBS ten times using rotator at 4°C and incubated with streptavidin conjugated with fluorescent dye Alexa Fluor™ 568 (Molecular Probes) with dilution 1:100 in filtered 1x PBS for 5 hours at room temperature. All stained tissues were then positioned muscular or mucosal side up on a glass slide and covered with coverslip 24 x 50 mm. In the first stained preparation, we found numerous randomly distributed oval solid artifacts. Optimization of staining procedure revealed that these artifacts attributable to the use of 1% goat blocking serum. In control experiments omitting goat serum eliminated these artifacts, while including goat serum reproduced them. Therefore, in all subsequent staining goat serum was omitted.

Visualization of reporter expression in sectioned and wholemount tissue

Images were taken with either Olympus FV1200 laser scanning confocal microscope or Andor Dragonfly spinning disk confocal microscope using Fusion software, and projection images were processed with Imaris software. In all cases the identification of anatomical structures and subnuclei were based on the mouse brain map (Paxinos and Franklin, 2012). Z stack images (10X and 20X) of the mouse esophagus and trachea (wholemount) were taken using Andor Dragonfly spinning disc microscope. Nerve terminals in the epithelial and subepithelial layers of the trachea were traced using Neurolucida 360 software (MBF Biosciences), as previously described (Dickstein et al., 2016): The 20X images were spaced at 0.6 µm. First, automatic nerve terminal detection (Rayburst crawl) was used, seeds were validated, then manual tracing was used to complete the tracing.

Vagal ganglia dissociation

Male 6-12-week-old $P2X_2$-tdTomato mice were euthanized by CO_2 asphyxiation followed by exsanguination. As previously described (Stanford and Taylor-Clark, 2018), vagal ganglia were

isolated in Ca^{2+}-free, Mg^{2+}-free Hank's buffered saline solution HBSS, then incubated in HBSS containing collagenase (2mg/ml) and dispase (2mg/ml), then mechanically dissociated with fire-polished pipettes. Individual neurons were washed with L-15 media supplemented with 10% fetal bovine serum, 100 U/ml penicillin and 100 µg/ml streptomycin then plated onto poly-D-lysine and laminin coated coverslips. Neurons were incubated at 37°C in antibiotic-free L-15 media supplemented with 10% fetal bovine serum and used within 24 hours.

Live neuron Ca^{2+} imaging and analysis

Neurons were incubated with 4µM FURA-2AM for 30-60 minutes at 37°C. Coverslips were loaded into a chamber on an inverted microscope and perfused with heated (33-34°C) HEPES buffer (154mM NaCl, 1.2mM KCl, 1.2mM $MgCl_2$, 2.5mM $CaCl_2$, 5.6mM D-Glucose). Slides equilibrated for 10 minutes prior to the start of the experiment and an image was taken to visualize tdTomato fluorescence (535nm excitation, 610nm emission). Changes in $[Ca^{2+}]_i$ was monitored using sequential excitation at 340nm and 380nm (510nm emission) with images taken every 6 seconds using a CoolSnap HQ2 camera (Photometrics) and evaluated ratiometrically using the 340/380 ratio. All drugs were diluted in HEPES buffer. αβmATP (10µM) was used to determine the functional expression of $P2X_{2/3}$ channels (Taylor-Clark et al., 2015). The EC_{50} for αβmATP-evoked activation of $P2X_{2/3}$ channels is ~3 to 9µM (Khakh et al., 2001; Liu et al., 2001). Capsaicin (1µM) was used to determine the functional expression of the nociceptive ion channel TRPV1 (Taylor-Clark et al., 2015). Neurons were further characterized by response to KCl (75mM) prior to ionomycin (5 µM), which evoked a maximal Ca^{2+} response. Image analysis was performed by using Nikon Elements (Nikon, Melville, NY) by drawing individual regions of interest (ROI) that around the intracellular region for each cell and tracked over time. ROI's with an unstable, high, or noisy baseline were eliminated from analysis. Neurons which failed to exhibit an increase in $[Ca^{2+}]_i$ to either αβmATP, capsaicin or KCl challenges (> 30% the ionomycin maximal response) were eliminated. Relative changes in $[Ca^{2+}]_i$ were determined ratiometrically using Fura-2 fluorescence: 340/380 ratio (R). This negates the impact of cell to cell variations in FURA-2AM loading. Data is presented as changes in the 340/380 ratio ($\Delta R = R_1 - R_0$), where R0 is the average 340/380 ratio prior to mATP treatment. As before (Stanford and Taylor-Clark, 2018; Stanford et al., 2019), an individual neuron was considered to be sensitive to a given agent if $R_{agent} > (R_{bl} + 2*SD_{bl}) + 0.075$; where R_{agent} is the average 340/380 ratio during treatment, R_{bl} is the average 340/380 ratio prior to treatment, and SD_{bl} is the standard deviation of R_{bl}. Neurons were grouped by tdTomato

expression and sensitivity to αβmATP and capsaicin. Data and statistical analyses were performed using Microsoft Excel and GraphPad Prism 7. Mean Ca^{2+} responses were compared using Student's T-test. A p value of 0.05 was taken as the threshold for significance.

Results

To investigate the expression of $P2X_2$, we generated a knockin $P2X_2^{Cre}$ mouse (Fig. 1) which was crossed with the cre-sensitive ROSA26-loxP-STOP-loxP-tdTomato reporter mouse. The resultant $P2X_2$-tdTomato mice express the red fluorescent tdTomato in $P2X_2$-expressing cells.

Cryostat sections of the vagal ganglia from 4 $P2X_2$-tdTomato mice showed robust and selective expression of tdTomato in nodose vagal sensory neurons, whereas there was little tdTomato expression in jugular vagal sensory neurons (1045 vs. 16 tdTomato+ neurons, respectively)(Fig. 2A). Vagal ganglia from 2 of these $P2X_2$-tdTomato mice were assessed for NeuroTrace™ (Nissl) staining (data not shown) to calculate the % of neurons that expressed tdTomato. More than 80% of nodose neurons were tdTomato+, compared to just 2% of jugular neurons (Fig. 3A). This is consistent with data from vagal ganglia from $P2X_2$-tdTomato stained for the neuronal marker pgp9.5, which again showed that few nodose neurons failed to express tdTomato (Fig. 2B). tdTomato expression in nodose neurons was noted in >75% of both TRPV1+ and TRPV1- populations (Figs. 2A-D, 3B). Very few tdTomato+ neurons also expressed TRKA, which was widely expressed in jugular neurons (Figs. 2C-D). We then investigated tdTomato expression in the trigeminal and thoracic DRG of $P2X_2$-tdTomato mice. In sections counterstained with NeuroTrace™, we found only 3.6% of trigeminal neurons were tdTomato+, and these were equally distributed between the maxillary/ophthalmic and mandibular regions (Figs. 2E-F, 3A). The rare tdTomato+ trigeminal neurons were mostly TRPV1+ (Figs. 2E-F, 3B). Few DRG neurons (12.3%) expressed tdTomato (Figs. 2G, 3A), although these were equally split between TRPV1+ and TRPV1- populations (Figs. 2G, 3B). Lastly, we found extensive tdTomato expression within the petrosal ganglia, with 75% of petrosal neurons from 4 ganglia expressing the marker (Fig. 2H).

To link tdTomato expression to $P2X_2$ expression in the $P2X_2$-tdTomato mouse, we investigated the sensitivity of vagal sensory neurons to the $P2X_{2/3}$ agonist αβmATP. Previous studies indicate that virtually all nodose and jugular neurons express $P2X_3$, but $P2X_2$ is only expressed in nodose neurons (Cockayne et al., 2005; Kwong et al., 2008; Nassenstein et al., 2010;

Surdenikova et al., 2012; Trancikova et al., 2018). αβmATP only causes significant vagal neuron activation in neurons that express both $P2X_2$ and $P2X_3$ (Lewis et al., 1995; Dunn et al., 2001; Khakh et al., 2001). Here, we assessed Ca^{2+} fluxes in dissociated $P2X_2$-tdTomato vagal neurons in response to αβmATP (10μM) and the TRPV1 agonist capsaicin (1μM) in 478 tdTomato+ and 200 tdTomato- neurons (Fig. 4). The mean response to αβmATP was significantly greater in tdTomato+ neurons compared to tdTomato- neurons (0.29±0.01 vs. 0.06±0.01, $p<0.05$). Out of the 478 tdTomato+ neurons, 399 neurons responded to αβmATP (83.4%)(Fig. 4C). Only 39 of the 200 tdTomato- neurons (19.5%) responded to αβmATP (Fig. 4C). The mean αβmATP response of αβmATP-sensitive neurons was greater in tdTomato+ neurons than tdTomato- neurons (0.35±0.01 vs. 0.22±0.04, $p<0.05$). There was no difference in mean capsaicin response between tdTomato+ and tdTomato- neurons (0.35±0.02 vs. 0.39±0.04, $p>0.05$). However, there were more capsaicin-sensitive neurons in the tdTomato+ population (261 out of 478, 54.6%) than in the tdTomato- population (72 out of 200, 36.0%). As such, the mean capsaicin response in capsaicin-sensitive neurons was significantly smaller in tdTomato+ neurons compared to tdTomato- neurons (0.66±0.03 vs. 1.08±0.09, $p<0.05$). Overall, the data indicate that tdTomato expression in vagal neurons of $P2X_2$-tdTomato mice is a selective marker of αβmATP sensitivity.

Sensory neurons in the vagal, petrosal and geniculate ganglia project central terminals via the tractus solitarius into the nTS in the brainstem medulla. In sections of the medulla of $P2X_2$-tdTomato mice, we found robust tdTomato expression in fibers within the tractus solitarius and the nTS, in particular in medial and dorsal subnuclei such as the commissural subnucleus (SolC), gelatinous subnucleus (SolG), dorsal lateral subnucleus (SolDL), medial subnucleus (SolM), intermediate subnucleus (SolIM) and central subnucleus (SolCe) (Fig. 5A-B). We also found some tdTomato+ fibers innervating the ventral subnucleus (SolV) and ventrolateral subnucleus (SolVL) and in the area postrema (Fig. 5B). These data are consistent with previous reports that nodose afferents innervate these medulla subnuclei (Kim et al., 2020). Previous studies have also shown that the central projections of TRPV1+ vagal afferents terminate mainly in the medial and dorsal nTS subnuclei and the area postrema (Kim et al., 2020). Here, we found substantial overlap of TRPV1 immunoreactivity and tdTomato within these areas, but the tdTomato+ fibers in lateral and ventral subnuclei did not express TRPV1, thus indicating that $P2X_2$+TRPV1+ and $P2X_2$+TRPV1- fibers have distinct central terminations (Fig. 5C), consistent with electrophysiological recordings of C- and A-fibers (Kubin et al., 1991; Kubin et al., 2006).

Serial sections indicated that tdTomato+ fibers were found along the entire rostral-caudal axis of the nTS (Fig. 5D). There was little tdTomato expression in the medulla other than within the tractus solitarius/nTS/area postrema. In particular, there were only a few sparse tdTomato+ terminations within the spinal trigeminal nucleus and the paratrigeminal complex, consistent with rare tdTomato expression in trigeminal afferent neurons. We did note tdTomato expression in minor subsets of neurons within the dorsal motor nucleus of the vagus and the external cuneate (Fig. 5B, D). Lastly, we found tdTomato+ neurons within the lateral reticular nucleus (Fig. 5D-G), which project mossy fibers to the cerebellum. Only a few tdTomato+ neurons were found in the neighboring caudal ventrolateral medulla (Fig. 5D-G). Almost none of the neurons in the rostral ventrolateral medulla expressed tdTomato (Fig. 5D). In the thoracic spinal cord, we observed some tdTomato+ fibers within the superficial laminae of the dorsal horn (Fig. 6) consistent with expression of tdTomato in a minor subset of DRG afferents. There was little tdTomato expression in other spinal areas.

We extended our investigation of tdTomato expression to the entire brain of $P2X_2$-tdTomato mice (Fig. 7). As expected, we again found tdTomato expression in the nTS and the lateral reticular nucleus. Interestingly, we also found tdTomato expression in a subset of neurons within the basal pontine nuclei (Fig. 7B, C), which also project mossy fibers to the cerebellum. Consistent with this, tdTomato+ mossy fiber axons within the white matter layer and mossy fiber terminations within the molecular layer were observed throughout each lobule of the cerebellum (Fig. 7D, E). In addition, a minor subset of cerebellar purkinje cells were tdTomato+ (Fig. 7F). No tdTomato+ neurons were observed in the deep cerebellar nuclei. We found very few neurons within the hippocampus expressed tdTomato (Fig. 7G, H), but some tdTomato+ fibers were noted within the molecular layer surrounding the dentate gyrus granule cell layer (Fig. 7I). In the cerebral cortex, tdTomato expression was found in a small number of pyramidal neurons, many of which were found in layer V and VI. In addition, a small number of neurons in the caudoputamen expressed tdTomato.

Next, we investigated tdTomato expression in the carotid body, tongue, trachea and esophagus – tissues that are thought to be innervated by $P2X_2$-expressing afferents (Rong et al., 2003; Finger et al., 2005; Yu et al., 2005; Kwong et al., 2008; Mazzone and Undem, 2016). In the carotid body, we observed dense terminations of glossopharyngeal tdTomato-expressing fibers innervating tyrosine hydroxylase-expressing glomus type 1 cells (Figs. 8A, B). We found tdTomato-expressing fibers innervating fungiform, filiform and circumvallate papillae on the

tongue (Figs. 8C, D, E). Intragemmal tdTomato+ terminations were observed in fungiform taste buds, along with the occasional perigemmal tdTomato+ terminations. In addition, tdTomato was observed in a subset of cells within the taste buds, which are likely taste cells (Huang et al., 2011). In wholemount preparations of the trachea we found tdTomato-expressing fibers throughout the entire trachea, although there were far more innervating the dorsal membranous part of the trachea (trachealis muscle regions) than in the anterolateral membranous parts over the cartilaginous rings and ligaments (not shown). In the membranous portion, tdTomato-expressing fibers were observed from the epithelial layer through to the adventitia (Fig. 8F). Distinct patterns of tdTomato-expressing fibers were noted in each layer. In the adventitia, dense cabling of fibers coursed parallel to the epithelial surface (Fig. 8G). In places, individual thin, punctate-like fibers were observed branching off the larger tdTomato-expressing axons that appeared to travel in bundles (Fig. 8G, insert). Multiple fibers climbed up to the smooth muscle layer, which was densely innervated with a host of parallel fibers following the transversal axis of the trachealis muscle (Fig. 8H). We found numerous tdTomato-expressing intraepithelial terminations within the membranous part of the trachea. These tended to have similar structures: parental axons proceeding up through the submucosal layer and then undergoing numerous branching in the subepithelial layer resulting in dense highly arborized structures intercalated with the tracheal epithelium (Figs. 8I, J). Nerve tracing software was able to show that each branch in the arbor was connected to the same parental axon, but we were unable to determine if the nearby arbors were derived from the same nerve. Lastly, we observed tdTomato-expressing fibers within the mucosal and submucosal layers of the esophagus (Fig. 8K). Often axons ran together through these layers in bundles of >5 axons, but individual punctate-like terminations could also be observed.

Lastly, we investigated the expression of tdTomato in the cochlea, based upon reports that $P2X_2$ is important for purinergic-mediated adaptation and protection against noise-induced ototoxicity (Yan et al., 2013; Cederholm et al., 2019). We found robust expression of tdTomato in numerous specialized cells within the organ of Corti, including in the inner hair cells, outer hair cells, Deiters cells, Hensen's cells and the outer pillar cells (Fig. 9). No tdTomato expression was noted in the basilar membrane. We also found tdTomato expression in the superficial interdental cells on the spiral limbus, and in some cells within the spiral ligament. Importantly, tdTomato was not found in any spiral sensory neurons within the spiral ganglia, nor in their fibers that innervate the hair cells.

Discussion

$P2X_2$ expression has previously been assessed in multiple cell types using immunohistochemistry, in situ hybridization, RT-PCR and functional sensitivity to ATP and other P2X ligands. Although it is generally agreed that $P2X_2$ is expressed on at least some peripheral afferent neurons, there is substantial disagreement regarding the precise details of its expression. Here, we have used a genetic approach, producing a knockin $P2X_2^{Cre}$ mouse that allows for the visualization of $P2X_2$ gene expression systematically. We replaced the endogenous $P2X_2$ stop codon with a 2A-Cre cassette. 2A is a self-cleaving peptide, thus expression of Cre recombinase peptides is expected to match $P2X_2$ peptide expression on a one-to-one basis. This gene-targeted Cre expression system is more efficient than internal ribosome entry site (IRES) sequences (Furler et al., 2001; Gao et al., 2012) that have often been used in other knockin Cre reporters.

The vagal ganglia are composed of nodose afferent neurons and jugular afferent neurons, both of which project sensory nerve terminals to multiple visceral organs. We found that almost all nodose neurons expressed tdTomato compared to almost none of the jugular neurons, thus indicating the selective expression of $P2X_2$ in the nodose portion of the vagal ganglia. Unlike in guinea pigs and larger mammals, the nodose and jugular ganglion are fused in mice. In these studies we have, based upon the idiosyncratic gross anatomy of each ganglion, subjectively assigned a hard line separating the nodose and jugular portions. This is likely an oversimplification of the distribution of nodose and jugular neurons, which are sometimes not perfectly delineated (Nassenstein et al., 2010; Surdenikova et al., 2012). As such, a small number of $P2X_2$+ and $P2X_2$- neurons may have been inappropriately assigned. Overall, our data are consistent with single neuron RT-PCR and RNA-seq analysis of nodose and jugular neurons which show that while $P2X_3$ is expressed by almost all vagal neurons, $P2X_2$ expression is restricted to nodose neurons (Kwong et al., 2008; Nassenstein et al., 2010; Surdenikova et al., 2012; Wang et al., 2017; Trancikova et al., 2018; Kupari et al., 2019). ATP or $\alpha\beta$mATP produces little to no activation of jugular afferents because of the rapid desensitization of homomeric $P2X_3$ channels, whereas these purinergic agonists evoke robust activation of dissociated nodose neurons and nodose peripheral terminals due to their persistent activation of heteromeric $P2X_{2/3}$ receptors (Undem et al., 2004; Yu et al., 2005; Kwong et al., 2008; Nassenstein et al., 2010). Indeed, knockout of $P2X_2$ converts ATP-evoked currents in nodose neurons into rapidly desensitizing $P2X_3$-like currents (Cockayne et al., 2005). We found that

Ca^{2+} influx responses to αβmATP in individual vagal neurons were correlated with tdTomato expression, confirming that the functional presence of $P2X_2$-like responses was consistent with $P2X_2$ reporter expression. $P2X_2$ expression was noted in both TRPV1+ and TRPV1- nodose populations, consistent with previous studies (Undem et al., 2004; Kwong et al., 2008; Taylor-Clark et al., 2015).

Compared to the vagal ganglia, there is greater uncertainty regarding the expression of $P2X_2$ in the DRG and trigeminal ganglia. $P2X_2$ immunoreactivity was reported to be in the majority of DRG neurons (Petruska et al., 2000b; Cockayne et al., 2005), and this immunoreactivity was absent in $P2X_2$ knockout mice (Cockayne et al., 2005). Nevertheless, using mixed or persistent ATP-evoked currents as a marker of $P2X_2$ expression, there are reports that $P2X_2$ expression ranges from ~10% to 50% of DRG neurons (Cockayne et al., 2000; Dunn et al., 2000; Petruska et al., 2000b; Petruska et al., 2000a; Cockayne et al., 2005). Our data indicates that ~12% of DRG neurons express $P2X_2$. This restricted expression is consistent with single neuron RT-PCR and RNA-seq analysis of DRG neurons (Kwong et al., 2008; Surdenikova et al., 2012; Usoskin et al., 2015; Hockley et al., 2018; Trancikova et al., 2018). $P2X_2$ immunoreactivity has also been reported to be in a large number of trigeminal neurons (Spehr et al., 2004; Ambalavanar et al., 2005; Simonetti et al., 2006; Staikopoulos et al., 2007). Mixed or persistent ATP-evoked currents have been noted in ~15 to 75% of trigeminal neurons (Spehr et al., 2004; Damann et al., 2006; Luo et al., 2006; Simonetti et al., 2006; Liu et al., 2015). Our data indicates that ~ 4% trigeminal neurons express $P2X_2$. It is possible that $P2X_2$'s contribution to 'persistent' ATP-evoked currents in trigeminal neurons has been overestimated due to context-dependent $P2X_3$ desensitization kinetics (Bianchi et al., 1999; Sokolova et al., 2006), and the contribution of other purinergic channels such as P2X1, P2X4 and P2X5, which are also expressed in trigeminal neurons (Kuroda et al., 2012; Liu et al., 2015).

Previous immunohistochemical and in situ hybridization studies have demonstrated widespread and robust $P2X_2$ expression throughout the rodent CNS, including in the nTS, area postrema, ventrolateral medulla, medial vestibular nucleus, spinal trigeminal nucleus, hippocampus, hypothalamus, thalamus, striatum, substantia nigra, cerebellum and cerebral cortex (Kidd et al., 1995; Collo et al., 1996; Vulchanova et al., 1996; Kanjhan et al., 1999; Yao et al., 2000; Gourine et al., 2003; Yao et al., 2003). However, based upon the inconsistencies of previous $P2X_2$ detection in sensory ganglia, we briefly investigated the CNS expression of $P2X_2$ with our reporter mouse. In general, we found $P2X_2$ expression in the CNS was limited compared to

previous reports. Consistent with the widespread expression of tdTomato in nodose and petrosal neurons we found tdTomato-expressing central terminals within multiple subnuclei throughout the nTS and in the area postrema. Thus $P2X_2$-expressing terminals target the same areas as terminals that express 5HT3 (another nodose neuronal marker that is expressed in very few jugular neurons) (Kim et al., 2020). The nTS is the major target of vagal, geniculate and petrosal ganglia afferents and is involved in reflex control of the cardiovascular, respiratory and digestive systems. Consistent with the expression of tdTomato in few trigeminal neurons, there was little tdTomato expression in the spinal trigeminal nucleus or the paratrigeminal complex in the medulla. This distinguishes the $P2X_2$-tdTomato expression observed here from 5HT3-tdTomato expression, as 5HT3 is expressed in a large number of trigeminal afferents (Kim et al., 2020). This suggests that vagal terminations in the paratrigeminal complex (Driessen et al., 2015; McGovern et al., 2015; Kim et al., 2020), which may play a role in defensive reflexes from the airways, are exclusively via jugular afferents. There was limited tdTomato expression in the thoracic spinal cord, with the majority observed in fibers terminating in the superficial laminae of the dorsal horn. These are most likely to be the central projections of the limited number of DRG afferents that express $P2X_2$.

There was little tdTomato expression throughout the rest of the brainstem, with the exception of a subset of neurons in the pontine nucleus and lateral reticular nucleus, both of which project glutamatergic mossy fibers to the cerebellum (Kratochwil et al., 2017). In particular, we found only sparse $P2X_2$ expression in the intermediate/caudal ventrolateral medulla and virtually no $P2X_2$ expression in the rostral ventrolateral medulla. Previous studies of ATP-evoked modulation of respiratory neurons within these regions have suggested that these actions correlated with $P2X_2$ immunoreactivity (Gourine et al., 2003; Yao et al., 2003). $P2X_2$ expression in mossy fibers has been reported previously (Collo et al., 1996; Kanjhan et al., 1999), and these channels are thought to be distributed along the projections to the cerebellum (Florenzano et al., 2002). Indeed, we observed robust tdTomato expression in a large number of mossy fibers within the cerebellum. tdTomato expression was limited in other brain regions to very few neurons. Of note, we found few $P2X_2$-expressing neurons within the hippocampus, despite immunohistochemical and in situ hybridization studies identifying widespread $P2X_2$ expression in neurons within the CA1-3 and dentate gyrus (Kidd et al., 1995; Kanjhan et al., 1999), and a transgenic mouse model with a $P2X_2$ fusion protein with yellow fluorescent protein identifying P2X expression in hippocampal mossy fibers (Haustein et al., 2014).

We exploited the robust expression of tdTomato throughout $P2X_2$-expressing peripheral nerves to study their anatomy. As expected, glossopharyngeal afferents (projected from petrosal neurons) innervating the glomus type 1 cells in the carotid body expressed $P2X_2$. Type 1 cells are the principle peripheral chemoreceptors, and $P2X_2$ receptors are required for hypoxic signaling (although not CO_2 detection) from the carotid body (Rong et al., 2003). The structural relationship between the $P2X_2$-expressing fibers and the Type 1 cells is consistent with previous immunohistochemical studies (Yokoyama et al., 2019). Gustatory afferents innervating taste buds in the tongue expressed $P2X_2$, consistent with the critical role of this receptor in taste cell-afferent signaling (Finger et al., 2005). Previous research has also shown $P2X_2$ expression in taste buds using RT-PCR, and signaling of taste cell $P2X_2$ may act as autocrine, positive feedback signal to amplify taste-evoked ATP secretion (Huang et al., 2011). Our data suggests that $P2X_2$ expression occurs in only a subset of taste cells.

We investigated $P2X_2$-expressing terminals in the trachea and esophagus, which are likely projected from nodose neurons (Ricco et al., 1996; Yu et al., 2005; Kwong et al., 2008; Prescott et al., 2020). Previous studies of vagal afferent terminations in the mouse trachea using GFP expression following intraganglionic injections of an AAV-GFP construct have identified two classes of vagal afferents in the membranous area of the trachea: dorsal terminal structures that had fibers running largely in parallel to the smooth muscle but did not penetrate the epithelial layer, and small intraepithelial terminals (Hennel et al., 2018). Based upon the similar morphology, it is likely that the $P2X_2$-expressing terminals observed in the trachea in the current study are a combination of dorsal terminal structures and small intraepithelial terminals, thus suggesting that these terminals are projected by nodose ($P2X_2$-expressing) neurons. Interestingly, the major vagal nerve terminal type found in the ligamentous part of the mouse trachea (termed 'anterolateral segmental array') by Hennel et al. (2018) was not labeled in $P2X_2$-tdTomato mice, indicating that these probably originate from jugular neurons. Previous tracheal studies have identified A-fiber terminals with complex dendritic arbors innervating the epithelium and subepithelial layers over the cartilage rings in rats (Yamamoto and Nakamuta, 2018) and in the subepithelial layer over the ends of the cartilage rings in guinea pigs (Mazzone et al., 2009). Despite the fact that tracheal A-fibers are likely projected from nodose neurons (Mazzone et al., 2009), they were not detected in either the present study in $P2X_2$-tdTomato mice or in the AAV-GFP mouse study by Hennel et al. (2018), suggesting species differences in A-fiber innervation of the trachea. This interpretation is somewhat complicated by the lack of $\alpha\beta$mATP sensitivity in nodose Aδ fibers innervating the guinea pig trachea (Canning et al.,

2004), suggesting that these nodose fibers surprisingly do not express $P2X_2$. However, there are no published reports of $P2X_2$ expression in guinea pig nodose neurons labeled from the trachea, so definitive conclusions are not possible at this time. We also observed tdTomato-expressing fibers in the esophageal mucosa, which is innervated by nodose, jugular and DRG afferents (Yu et al., 2005; Surdenikova et al., 2012; Ru et al., 2015). Similar nerve structures were identified in the mouse esophageal mucosa following vagal intraganglionic injections of AAV-GFP (Harsanyiova et al., 2020). Thus, it is likely that the esophageal fibers identified here are projected by nodose ($P2X_2$-expressing) neurons.

Lastly, we found evidence of $P2X_2$ expression in hair cells and their support cells within the organ of Corti in the cochlea. Previous studies have shown that both inner and outer hair cells express $P2X_2$ which mediate ATP-induced cationic currents (Housley et al., 1999; Järlebark et al., 2002). We found no expression of $P2X_2$ in the spiral ganglionic afferents that innervate the inner and outer hair cells, in disagreement with some immunohistochemical studies and dissociated patch clamp studies (Järlebark et al., 2002; Weisz et al., 2009; Ito and Dulon, 2010). Knockout of $P2X_2$ has no effect on auditory thresholds in non-aged mice (Yan et al., 2013), indicating that this channel is not critical to neurotransmission between the inner hair cells and the type I spiral afferents. Nevertheless, $P2X_2$ knockout accelerates noise-induced ototoxicity (Yan et al., 2013). Noise evokes local ATP release which causes $P2X_2$-mediated dampening of the cochlea amplifier by modifying the electromotility properties of the outer hair cells (Yu and Zhao, 2008; Housley et al., 2013; Cederholm et al., 2019). This paracrine humeral purinergic signaling is thought to complement the medial olivocochlear reflex suppression of the cochlear amplifier that is mediated by the type 2 spiral afferents that innervate the outer hair cells (Froud et al., 2015). Our observation of $P2X_2$ only in the hair cells and support cells is consistent with recent research that directly implicated the outer hair cell rather than the spiral afferents in the $P2X_2$-mediated pathways (Cederholm et al., 2019).

In summary, the $P2X_2$-cre reporter mouse demonstrates that $P2X_2$ expression is limited to subsets of neurons and specialized cells in the cochlea. Previous reports using biochemical techniques have overestimated the number of cell types that express $P2X_2$. This mouse provides a genetic approach to the identification and manipulation of $P2X_2$-expressing cell types. The current study used ROSA26-loxP-STOP-loxP-tdTomato mice to visualize cre-mediated recombination in the $P2X_2$-cre expressing cells. It should be noted that the excision of the loxP-flanked stop region upon cre expression is irreversible, thus tdTomato expression

cannot discriminate between transient and current $P2X_2$ expression in a given cell. It is possible that some of the tdTomato expression described here is due to transient $P2X_2$ expression.

Legends

Figure 1: Development of the knockin $P2X_2^{Cre}$ mouse. A, targeting strategy for the replacement of the $P2X_2$ TGA stop codon with a 2A-Cre cassette (2A self-cleaving peptide in purple, Cre in dark grey). Homology arms (blue and red lines) were generated for the P2X2 gene (exons, 5' and 3' untranslated regions (UTR) in orange) and the latter portion of the neighboring Pole gene (exons, and 3' UTR in green). Homology arms of targeting vector include a neomycin resistance gene (Neo^R) flanked by self-deletion anchor (SDA) sites for positive selection. A Diphtheria toxin A fragment gene (DTA) was placed in a non-homologous region of targeting vector as a negative selection for non-homologous recombination. B, PCR of $P2X_2$ gene in offspring from a pairing of heterozygous $P2X_2^{Cre}$ mice. As expected, offspring have a mendelian distribution of mutant (i.e. $P2X_2^{Cre}$, at 394 bp) and wildtype (at 319 bp) alleles.

Figure 2: tdTomato expression in $P2X_2$-tdTomato mice is restricted to subsets of sensory afferents. A to C, tdTomato (red) expression in vagal ganglia, with the demarcation of the nodose and jugular regions delineated by dotted line. A, counterstained for TRPV1 (green) expression. B, counterstained for TRPV1 (blue) and pgp9.5 (green) expression. C, counterstained for TRPV1 (blue) and TRKA (green) expression. D, tdTomato (red) expression in nodose neurons identified in C. *Left*, counterstained for TRPV1 (green) expression; *Middle*, counterstained for TRKA (green) expression; *Right*, counterstained for TRPV1 (blue) and TRKA (green) expression. E to G, tdTomato (red) expression counterstained for TRPV1 expression (blue) and with NeuroTrace™ (green). E, maxillary/ophthalmic region of the trigeminal ganglia. tdTomato+ neurons identified by white arrows. F, mandibular region of the trigeminal ganglia. G, DRG. H, Petrosal ganglia, counterstained with NeuroTrace™ (green). Scale bars denotes 100μm (A, B, C and E), 50μm (D, F and G) or 20μm (H). Data is derived from 5 vagal ganglia, 5 trigeminal ganglia, 4 DRG and 4 petrosal ganglia.

Figure 3: Quantification of tdTomato and TRPV1 expression in vagal, trigeminal and DRG afferents. A, the % of neurotrace+ neurons that express tdTomato and TRPV1. B, the % of TRPV1+ neurons and TRPV1- neurons that also express tdTomato. Data is derived from 2 vagal ganglia, 5 trigeminal ganglia and 3 thoracic DRG.

Figure 4: Responsivity to αβmATP correlates with reporter expression in vagal neurons from $P2X_2$-tdTomato mice. A, brightfield image of dissociated vagal neurons overlaid with tdTomato (red) expression. Scale bar denotes 40μm. B, mean +/- SEM $[Ca^{2+}]_i$ responses of tdTomato+ (red, n=478) and tdTomato- (black, n=200) vagal neurons to αβmATP (10μM), capsaicin (Caps, 1μM) and KCl (75mM). C, Euler diagram denoting the number of vagal neurons in each specific subset as determined by tdTomato expression and responsivity to αβmATP and capsaicin.

Figure 5: tdTomato expression in the medulla of $P2X_2$-tdTomato mice. A and B, tdTomato (red) expression in the dorsal medulla counterstained with NeuroTrace™ (green). A, sagittal section at midline. B, coronal section at -300μm (relative to obex). C, tdTomato (red) expression counterstained for TRPV1 (green) expression in coronal section at -390μm (relative to obex). D, tdTomato expression in serial coronal sections from rostral to caudal, with labeling for the position relative to obex. The intensity of native tdTomato expression is shown in rainbow pseudocolor. E to G, tdTomato (red) expression in the ventrolateral medulla counterstained with NeuroTrace™ (green). E, coronal section at -540μm (relative to obex). F, higher magnification of insert in E. G, sagittal section at 1.08mm lateral to midline. The following structures are identified: area postrema (AP), central canal (CC), external cuneate nucleus (ECu), dorsal motor nucleus of the vagus (DMX), hypoglossal motor nucleus (12N), lateral reticular nucleus (LRt), nucleus tractus solitarius (NTS), SolC (C), SolCe (Ce), SolDL (DL), SolG (G), SolIM (IM), SolM (M), SolV (V), SolVL (VL) and tractus solitarius (TS). Scale bars denotes 50μm (A), 300μm (B and C) or 500μm (D).

Figure 6: tdTomato expression in the thoracic spinal cord of $P2X_2$-tdTomato mice. A and B, Coronal sections with tdTomato expression (red), with (A) and without (B) counterstain by NeuroTrace™ (green). C, higher magnification of superficial dorsal horn laminae. Scale bars denotes 100μm (A and B) or 50μm (C).

Figure 7: tdTomato expression within the brainstem and brain of $P2X_2$-tdTomato mice. A, tdTomato (white) expression in sagittal section at 1mm lateral to the midline. Ecu, external cuneate nucleus; NTS, nucleus tractus solitarius. B to L, tdTomato (red) expression counterstained with NeuroTrace™ (green). B, basal pontine nucleus. C, high magnification of area identified in B. D, cerebellum. E, high magnification of area identified in D showing white

matter and internal granule layer. F, high magnification of area identified in D showing internal granule layer, purkinje cells and the molecular layer. G, hippocampus. DG, dentate gyrus. H, suprapyramidal blade of the dentate gyrus. GC layer, granular cell layer. I, apex of the dentate gyrus. J, cerebral cortex, insert shows tdTomato expression without NeuroTrace™. L5, layer 5; L6, layer 6; WM, white matter. K and L, caudoputamen with (H) and without (I) NeuroTrace™. Scale bars denotes 2mm (A), 400μm (D), 300μm (G), 100μm (B and J), 80μm (H and I), 60μm (C, F, K and L), 50μm (J insert) or 40μm (E).

Figure 8: tdTomato expression in nerves innervating carotid bodies, taste buds, trachea and esophagus of $P2X_2$-tdTomato mice. A, carotid body type 1 cells expressing tyrosine hydroxylase (green) are innervated by nerves expressing tdTomato (red). B, higher magnification of area identified in A. C-E, taste bud on the surface of the tongue is innervated by nerves expressing tdTomato (red). Dapi staining (blue) identifies cell nuclei. D and E, higher magnification of area identified in C. Arrowhead denotes intragemmal fibers, arrow denotes perigemmal fiber. Note the expression of tdTomato in a subset of taste cells within the taste bud. F-J, tdTomato-expressing fibers throughout the epithelial, submucosal, trachealis muscle and adventitial layers in a wholemount preparation of the trachea. F, complete z projection, with tdTomato expression pseudocolor indicating the z depth (total of 182μm). G, extensive cabling of tdTomato-expressing fibers (red) in the adventitial layer with some of the muscle layer (63μm in depth). Insert, higher magnification of area identified in G. Arrowhead highlights an example of a punctate multi-branched fiber branching off a thick bundle of broad axons. H, tdTomato-expressing fibers (red) innervating the trachealis muscle layer (25μm in depth). I and J, tdTomato-expressing intraepithelial terminations (red) within the epithelial layer. Terminal arborizations were traced using Neurolucida software (J). K, tdTomato-expressing fibers (red) in the submucosa and mucosal muscle layers in a wholemount preparation of the esophagus. Scale bars denotes 100μm (A, C, F, G, H, I, J, K) or 30μm (B, D, E, G insert).

Figure 9: tdTomato expression within the cochlear of $P2X_2$-tdTomato mice. A, section with tdTomato expression (red) including afferent cell bodies in the spiral ganglion, the spiral limbus, spiral ligament and the organ of Corti, counterstained with NeuroTrace™ (green) and DAPI (blue). The tectorial membrane is missing from this section. B, higher magnification of the organ of Corti from A. The following additional structures are identified: basilar membrane (BM), inner

669 hair cells (IHC), outer hair cells (OHC), outer pillar cells (OPC). Scale bars denotes 100μm (A)
670 or 30μm (B).
671
672
673

674 References

675

676 Ambalavanar R, Moritani M, Dessem D (2005) Trigeminal P2X3 receptor expression differs from
677 dorsal root ganglion and is modulated by deep tissue inflammation. Pain 117:280-291.
678 Bianchi BR, Lynch KJ, Touma E, Niforatos W, Burgard EC, Alexander KM, Park HS, Yu H,
679 Metzger R, Kowaluk E, Jarvis MF, van Biesen T (1999) Pharmacological
680 characterization of recombinant human and rat P2X receptor subtypes. Eur J Pharmacol
681 376:127-138.
682 Brake AJ, Wagenbach MJ, Julius D (1994) New structural motif for ligand-gated ion channels
683 defined by an ionotropic ATP receptor. Nature 371:519-523.
684 Canning BJ, Mazzone SB, Meeker SN, Mori N, Reynolds SM, Undem BJ (2004) Identification of
685 the tracheal and laryngeal afferent neurones mediating cough in anaesthetized guinea-
686 pigs. J Physiol 557:543-558.
687 Cederholm JME, Ryan AF, Housley GD (2019) Onset kinetics of noise-induced purinergic
688 adaptation of the 'cochlear amplifier'. Purinergic signalling 15:343-355.
689 Chen CC, Akopian AN, Sivilotti L, Colquhoun D, Burnstock G, Wood JN (1995) A P2X
690 purinoceptor expressed by a subset of sensory neurons. Nature 377:428-431.
691 Cockayne DA, Dunn PM, Zhong Y, Rong W, Hamilton SG, Knight GE, Ruan HZ, Ma B, Yip P,
692 Nunn P, McMahon SB, Burnstock G, Ford AP (2005) P2X2 knockout mice and
693 P2X2/P2X3 double knockout mice reveal a role for the P2X2 receptor subunit in
694 mediating multiple sensory effects of ATP. J Physiol 567:621-639.
695 Cockayne DA, Hamilton SG, Zhu QM, Dunn PM, Zhong Y, Novakovic S, Malmberg AB, Cain G,
696 Berson A, Kassotakis L, Hedley L, Lachnit WG, Burnstock G, McMahon SB, Ford AP
697 (2000) Urinary bladder hyporeflexia and reduced pain-related behaviour in P2X3-
698 deficient mice. Nature 407:1011-1015.
699 Collo G, North RA, Kawashima E, Merlo-Pich E, Neidhart S, Surprenant A, Buell G (1996)
700 Cloning of P2X5 and P2X6 receptors and the distribution and properties of an extended
701 family of ATP-gated ion channels. J Neurosci 16:2495-2507.
702 Damann N, Rothermel M, Klupp BG, Mettenleiter TC, Hatt H, Wetzel CH (2006) Chemosensory
703 properties of murine nasal and cutaneous trigeminal neurons identified by viral tracing.
704 BMC Neurosci 7:46.
705 Dickstein DL, Dickstein DR, Janssen WG, Hof PR, Glaser JR, Rodriguez A, O'Connor N,
706 Angstman P, Tappan SJ (2016) Automatic Dendritic Spine Quantification from Confocal
707 Data with Neurolucida 360. Current protocols in neuroscience 77:1.27.21-21.27.21.

708 Driessen AK, Farrell MJ, Mazzone SB, McGovern AE (2015) The Role of the Paratrigeminal
709 Nucleus in Vagal Afferent Evoked Respiratory Reflexes: A Neuroanatomical and
710 Functional Study in Guinea Pigs. Front Physiol 6:378.
711 Dunn PM, Zhong Y, Burnstock G (2001) P2X receptors in peripheral neurons. Prog Neurobiol
712 65:107-134.
713 Dunn PM, Liu M, Zhong Y, King BF, Burnstock G (2000) Diinosine pentaphosphate: an
714 antagonist which discriminates between recombinant P2X(3) and P2X(2/3) receptors
715 and between two P2X receptors in rat sensory neurones. Br J Pharmacol 130:1378-
716 1384.
717 Finger TE, Danilova V, Barrows J, Bartel DL, Vigers AJ, Stone L, Hellekant G, Kinnamon SC
718 (2005) ATP signaling is crucial for communication from taste buds to gustatory nerves.
719 Science 310:1495-1499.
720 Florenzano F, Viscomi MT, Cavaliere F, Volonte C, Molinari M (2002) Cerebellar lesion up-
721 regulates P2X1 and P2X2 purinergic receptors in precerebellar nuclei. Neuroscience
722 115:425-434.
723 Froud KE, Wong AC, Cederholm JM, Klugmann M, Sandow SL, Julien JP, Ryan AF, Housley
724 GD (2015) Type II spiral ganglion afferent neurons drive medial olivocochlear reflex
725 suppression of the cochlear amplifier. Nat Commun 6:7115.
726 Furler S, Paterna JC, Weibel M, Bueler H (2001) Recombinant AAV vectors containing the foot
727 and mouth disease virus 2A sequence confer efficient bicistronic gene expression in
728 cultured cells and rat substantia nigra neurons. Gene therapy 8:864-873.
729 Gao SY, Jack MM, O'Neill C (2012) Towards optimising the production of and expression from
730 polycistronic vectors in embryonic stem cells. PLoS One 7:e48668.
731 Gourine AV, Atkinson L, Deuchars J, Spyer KM (2003) Purinergic signalling in the medullary
732 mechanisms of respiratory control in the rat: respiratory neurones express the P2X2
733 receptor subunit. J Physiol 552:197-211.
734 Harsanyiova J, Ru F, Zatko T, Kollarik M, Hennel M (2020) Vagus Nerves Provide a Robust
735 Afferent Innervation of the Mucosa Throughout the Body of the Esophagus in the Mouse.
736 Dysphagia 35:471-478.
737 Haustein MD, Kracun S, Lu XH, Shih T, Jackson-Weaver O, Tong X, Xu J, Yang XW, O'Dell TJ,
738 Marvin JS, Ellisman MH, Bushong EA, Looger LL, Khakh BS (2014) Conditions and
739 constraints for astrocyte calcium signaling in the hippocampal mossy fiber pathway.
740 Neuron 82:413-429.

741 Hennel M, Harsanyiova J, Ru F, Zatko T, Brozmanova M, Trancikova A, Tatar M, Kollarik M
742 (2018) Structure of vagal afferent nerve terminal fibers in the mouse trachea. Respir
743 Physiol Neurobiol 249:35-46.
744 Hockley JRF, Taylor TS, Callejo G, Wilbrey AL, Gutteridge A, Bach K, Winchester WJ, Bulmer
745 DC, McMurray G, Smith ESJ (2018) Single-cell RNAseq reveals seven classes of
746 colonic sensory neuron. Gut.
747 Housley GD, Morton-Jones R, Vlajkovic SM, Telang RS, Paramananthasivam V, Tadros SF,
748 Wong AC, Froud KE, Cederholm JM, Sivakumaran Y, Snguanwongchai P, Khakh BS,
749 Cockayne DA, Thorne PR, Ryan AF (2013) ATP-gated ion channels mediate adaptation
750 to elevated sound levels. Proc Natl Acad Sci U S A 110:7494-7499.
751 Housley GD, Kanjhan R, Raybould NP, Greenwood D, Salih SG, Järlebark L, Burton LD, Setz
752 VC, Cannell MB, Soeller C, Christie DL, Usami S, Matsubara A, Yoshie H, Ryan AF,
753 Thorne PR (1999) Expression of the P2X(2) receptor subunit of the ATP-gated ion
754 channel in the cochlea: implications for sound transduction and auditory
755 neurotransmission. J Neurosci 19:8377-8388.
756 Huang YA, Stone LM, Pereira E, Yang R, Kinnamon JC, Dvoryanchikov G, Chaudhari N, Finger
757 TE, Kinnamon SC, Roper SD (2011) Knocking out P2X receptors reduces transmitter
758 secretion in taste buds. J Neurosci 31:13654-13661.
759 Ito K, Dulon D (2010) Purinergic signaling in cochleovestibular hair cells and afferent neurons.
760 Purinergic signalling 6:201-209.
761 Järlebark LE, Housley GD, Raybould NP, Vlajkovic S, Thorne PR (2002) ATP-gated ion
762 channels assembled from P2X2 receptor subunits in the mouse cochlea. Neuroreport
763 13:1979-1984.
764 Kanjhan R, Housley GD, Burton LD, Christie DL, Kippenberger A, Thorne PR, Luo L, Ryan AF
765 (1999) Distribution of the P2X2 receptor subunit of the ATP-gated ion channels in the rat
766 central nervous system. J Comp Neurol 407:11-32.
767 Khakh BS, Burnstock G, Kennedy C, King BF, North RA, Seguela P, Voigt M, Humphrey PP
768 (2001) International union of pharmacology. XXIV. Current status of the nomenclature
769 and properties of P2X receptors and their subunits. Pharmacol Rev 53:107-118.
770 Kidd EJ, Grahames CB, Simon J, Michel AD, Barnard EA, Humphrey PP (1995) Localization of
771 P2X purinoceptor transcripts in the rat nervous system. Mol Pharmacol 48:569-573.
772 Kim SH, Hadley SH, Maddison M, Patil M, Cha BJ, Kollarik M, Taylor-Clark TE (2020) Mapping
773 of sensory nerve subsets within the vagal ganglia and the brainstem using reporter mice
774 for Pirt, TRPV1, 5HT3 and Tac1 expression. eNeuro.

775 Kratochwil CF, Maheshwari U, Rijli FM (2017) The Long Journey of Pontine Nuclei Neurons:
776 From Rhombic Lip to Cortico-Ponto-Cerebellar Circuitry. Frontiers in neural circuits
777 11:33.
778 Kubin L, Kimura H, Davies RO (1991) The medullary projections of afferent bronchopulmonary
779 C fibres in the cat as shown by antidromic mapping. J Physiol 435:207-228.
780 Kubin L, Alheid GF, Zuperku EJ, McCrimmon DR (2006) Central pathways of pulmonary and
781 lower airway vagal afferents. J Appl Physiol 101:618-627.
782 Kupari J, Haring M, Agirre E, Castelo-Branco G, Ernfors P (2019) An Atlas of Vagal Sensory
783 Neurons and Their Molecular Specialization. Cell Rep 27:2508-2523.e2504.
784 Kuroda H, Shibukawa Y, Soya M, Masamura A, Kasahara M, Tazaki M, Ichinohe T (2012)
785 Expression of P2X(1) and P2X(4) receptors in rat trigeminal ganglion neurons.
786 Neuroreport 23:752-756.
787 Kwong K, Kollarik M, Nassenstein C, Ru F, Undem BJ (2008) P2X2 Receptors Differentiate
788 Placodal vs Neural Crest C-fiber Phenotypes Innervating Guinea Pig Lungs and
789 Esophagus. Am J Physiol Lung Cell Mol Physiol 295:L858-865.
790 Lewis C, Neidhart S, Holy C, North RA, Buell G, Surprenant A (1995) Coexpression of P2X2
791 and P2X3 receptor subunits can account for ATP-gated currents in sensory neurons.
792 Nature 377:432-435.
793 Liu M, King BF, Dunn PM, Rong W, Townsend-Nicholson A, Burnstock G (2001) Coexpression
794 of P2X(3) and P2X(2) receptor subunits in varying amounts generates heterogeneous
795 populations of P2X receptors that evoke a spectrum of agonist responses comparable to
796 that seen in sensory neurons. J Pharmacol Exp Ther 296:1043-1050.
797 Liu Y, Tian X, Wu Y, Chen L, Yi CL, Li ZW, Zhang Y, Li CY (2015) Phenotypes of ATP-activated
798 current associated with their genotypes of P2X1-6 subunits in neurons innervating tooth-
799 pulp. Biochem Biophys Res Commun 458:596-600.
800 Luo J, Yin GF, Gu YZ, Liu Y, Dai JP, Li C, Li ZW (2006) Characterization of three types of ATP-
801 activated current in relation to P2X subunits in rat trigeminal ganglion neurons. Brain
802 Res 1115:9-15.
803 Mazzone SB, Undem BJ (2016) Vagal Afferent Innervation of the Airways in Health and
804 Disease. Physiol Rev 96:975-1024.
805 Mazzone SB, Reynolds SM, Mori N, Kollarik M, Farmer DG, Myers AC, Canning BJ (2009)
806 Selective expression of a sodium pump isozyme by cough receptors and evidence for its
807 essential role in regulating cough. J Neurosci 29:13662-13671.

McCord JL, Tsuchimochi H, Kaufman MP (2010) P2X2/3 and P2X3 receptors contribute to the metaboreceptor component of the exercise pressor reflex. J Appl Physiol (1985) 109:1416-1423.

McGovern AE, Driessen AK, Simmons DG, Powell J, Davis-Poynter N, Farrell MJ, Mazzone SB (2015) Distinct brainstem and forebrain circuits receiving tracheal sensory neuron inputs revealed using a novel conditional anterograde transsynaptic viral tracing system. J Neurosci 35:7041-7055.

Nassenstein C, Taylor-Clark TE, Myers AC, Ru F, Nandigama R, Bettner W, Undem BJ (2010) Phenotypic distinctions between neural crest and placodal derived vagal C-fibres in mouse lungs. J Physiol 588:4769-4783.

Paxinos G, Franklin B (2012) Mouse Brain in Stereotaxic Coordinates, 4th Edition Edition: Elsevier.

Petruska JC, Cooper BY, Johnson RD, Gu JG (2000a) Distribution patterns of different P2x receptor phenotypes in acutely dissociated dorsal root ganglion neurons of adult rats. Exp Brain Res 134:126-132.

Petruska JC, Cooper BY, Gu JG, Rau KK, Johnson RD (2000b) Distribution of P2X1, P2X2, and P2X3 receptor subunits in rat primary afferents: relation to population markers and specific cell types. J Chem Neuroanat 20:141-162.

Prescott SL, Umans BD, Williams EK, Brust RD, Liberles SD (2020) An Airway Protection Program Revealed by Sweeping Genetic Control of Vagal Afferents. Cell 181:574-589.e514.

Ricco MM, Kummer W, Biglari B, Myers AC, Undem BJ (1996) Interganglionic segregation of distinct vagal afferent fibre phenotypes in guinea-pig airways. J Physiol 496 (Pt 2):521-530.

Rong W, Gourine AV, Cockayne DA, Xiang Z, Ford AP, Spyer KM, Burnstock G (2003) Pivotal role of nucleotide P2X2 receptor subunit of the ATP-gated ion channel mediating ventilatory responses to hypoxia. J Neurosci 23:11315-11321.

Ru F, Banovcin P, Jr., Kollarik M (2015) Acid sensitivity of the spinal dorsal root ganglia C-fiber nociceptors innervating the guinea pig esophagus. Neurogastroenterol Motil 27:865-874.

Simonetti M, Fabbro A, D'Arco M, Zweyer M, Nistri A, Giniatullin R, Fabbretti E (2006) Comparison of P2X and TRPV1 receptors in ganglia or primary culture of trigeminal neurons and their modulation by NGF or serotonin. Mol Pain 2:11.

Sokolova E, Skorinkin A, Moiseev I, Agrachev A, Nistri A, Giniatullin R (2006) Experimental and modeling studies of desensitization of P2X3 receptors. Mol Pharmacol 70:373-382.

842 Song X, Gao X, Guo D, Yu Q, Guo W, He C, Burnstock G, Xiang Z (2012) Expression of P2X(2)
843 and P2X (3) receptors in the rat carotid sinus, aortic arch, vena cava, and heart, as well
844 as petrosal and nodose ganglia. Purinergic signalling 8:15-22.
845 Spehr J, Spehr M, Hatt H, Wetzel CH (2004) Subunit-specific P2X-receptor expression defines
846 chemosensory properties of trigeminal neurons. Eur J Neurosci 19:2497-2510.
847 Staikopoulos V, Sessle BJ, Furness JB, Jennings EA (2007) Localization of P2X2 and P2X3
848 receptors in rat trigeminal ganglion neurons. Neuroscience 144:208-216.
849 Stanford KR, Taylor-Clark TE (2018) Mitochondrial modulation-induced activation of vagal
850 sensory neuronal subsets by antimycin A, but not CCCP or rotenone, correlates with
851 mitochondrial superoxide production. PLoS One 13:e0197106.
852 Stanford KR, Hadley SH, Barannikov I, Ajmo JM, Bahia PK, Taylor-Clark TE (2019) Antimycin
853 A-induced mitochondrial dysfunction activates vagal sensory neurons via ROS-
854 dependent activation of TRPA1 and ROS-independent activation of TRPV1. Brain Res
855 1715:94-105.
856 Surdenikova L, Ru F, Nassenstein C, Tatar M, Kollarik M (2012) The neural crest- and
857 placodes-derived afferent innervation of the mouse esophagus. Neurogastroenterol Motil
858 24:e517-525.
859 Taylor-Clark TE, Wu KY, Thompson JA, Yang K, Bahia PK, Ajmo JM (2015) Thy1.2 YFP-16
860 transgenic mouse labels a subset of large-diameter sensory neurons that lack TRPV1
861 expression. PLoS One 10:e0119538.
862 Trancikova A, Kovacova E, Ru F, Varga K, Brozmanova M, Tatar M, Kollarik M (2018) Distinct
863 Expression of Phenotypic Markers in Placodes- and Neural Crest-Derived Afferent
864 Neurons Innervating the Rat Stomach. Dig Dis Sci 63:383-394.
865 Undem BJ, Chuaychoo B, Lee MG, Weinreich D, Myers AC, Kollarik M (2004) Subtypes of
866 vagal afferent C-fibres in guinea-pig lungs. J Physiol 556:905-917.
867 Usoskin D, Furlan A, Islam S, Abdo H, Lonnerberg P, Lou D, Hjerling-Leffler J, Haeggstrom J,
868 Kharchenko O, Kharchenko PV, Linnarsson S, Ernfors P (2015) Unbiased classification
869 of sensory neuron types by large-scale single-cell RNA sequencing. Nat Neurosci
870 18:145-153.
871 Vulchanova L, Arvidsson U, Riedl M, Wang J, Buell G, Surprenant A, North RA, Elde R (1996)
872 Differential distribution of two ATP-gated channels (P2X receptors) determined by
873 immunocytochemistry. Proc Natl Acad Sci U S A 93:8063-8067.
874 Wang J, Kollarik M, Ru F, Sun H, McNeil B, Dong X, Stephens G, Korolevich S, Brohawn P,
875 Kolbeck R, Undem B (2017) Distinct and common expression of receptors for

876 inflammatory mediators in vagal nodose versus jugular capsaicin-sensitive/TRPV1-
877 positive neurons detected by low input RNA sequencing. PLoS One 12:e0185985.
878 Weigand LA, Ford AP, Undem BJ (2012) A role for ATP in bronchoconstriction-induced
879 activation of guinea pig vagal intrapulmonary C-fibres. J Physiol 590:4109-4120.
880 Weisz C, Glowatzki E, Fuchs P (2009) The postsynaptic function of type II cochlear afferents.
881 Nature 461:1126-1129.
882 Yamamoto Y, Nakamuta N (2018) Morphology of P2X3-immunoreactive nerve endings in the rat
883 tracheal mucosa. J Comp Neurol 526:550-566.
884 Yan D et al. (2013) Mutation of the ATP-gated P2X(2) receptor leads to progressive hearing
885 loss and increased susceptibility to noise. Proc Natl Acad Sci U S A 110:2228-2233.
886 Yao ST, Barden JA, Finkelstein DI, Bennett MR, Lawrence AJ (2000) Comparative study on the
887 distribution patterns of P2X(1)-P2X(6) receptor immunoreactivity in the brainstem of the
888 rat and the common marmoset (Callithrix jacchus): association with catecholamine cell
889 groups. J Comp Neurol 427:485-507.
890 Yao ST, Gourine AV, Spyer KM, Barden JA, Lawrence AJ (2003) Localisation of P2X2 receptor
891 subunit immunoreactivity on nitric oxide synthase expressing neurones in the brain stem
892 and hypothalamus of the rat: a fluorescence immunohistochemical study. Neuroscience
893 121:411-419.
894 Yokoyama T, Settai K, Nakamuta N, Yamamoto Y (2019) Distribution and morphology of
895 baroreceptors in the rat carotid sinus as revealed by immunohistochemistry for P2X3
896 purinoceptors. Histochem Cell Biol 151:161-173.
897 Yu N, Zhao HB (2008) ATP activates P2x receptors and requires extracellular Ca(++)
898 participation to modify outer hair cell nonlinear capacitance. Pflugers Arch 457:453-461.
899 Yu S, Undem BJ, Kollarik M (2005) Vagal afferent nerves with nociceptive properties in guinea-
900 pig oesophagus. J Physiol 563:831-842.
901

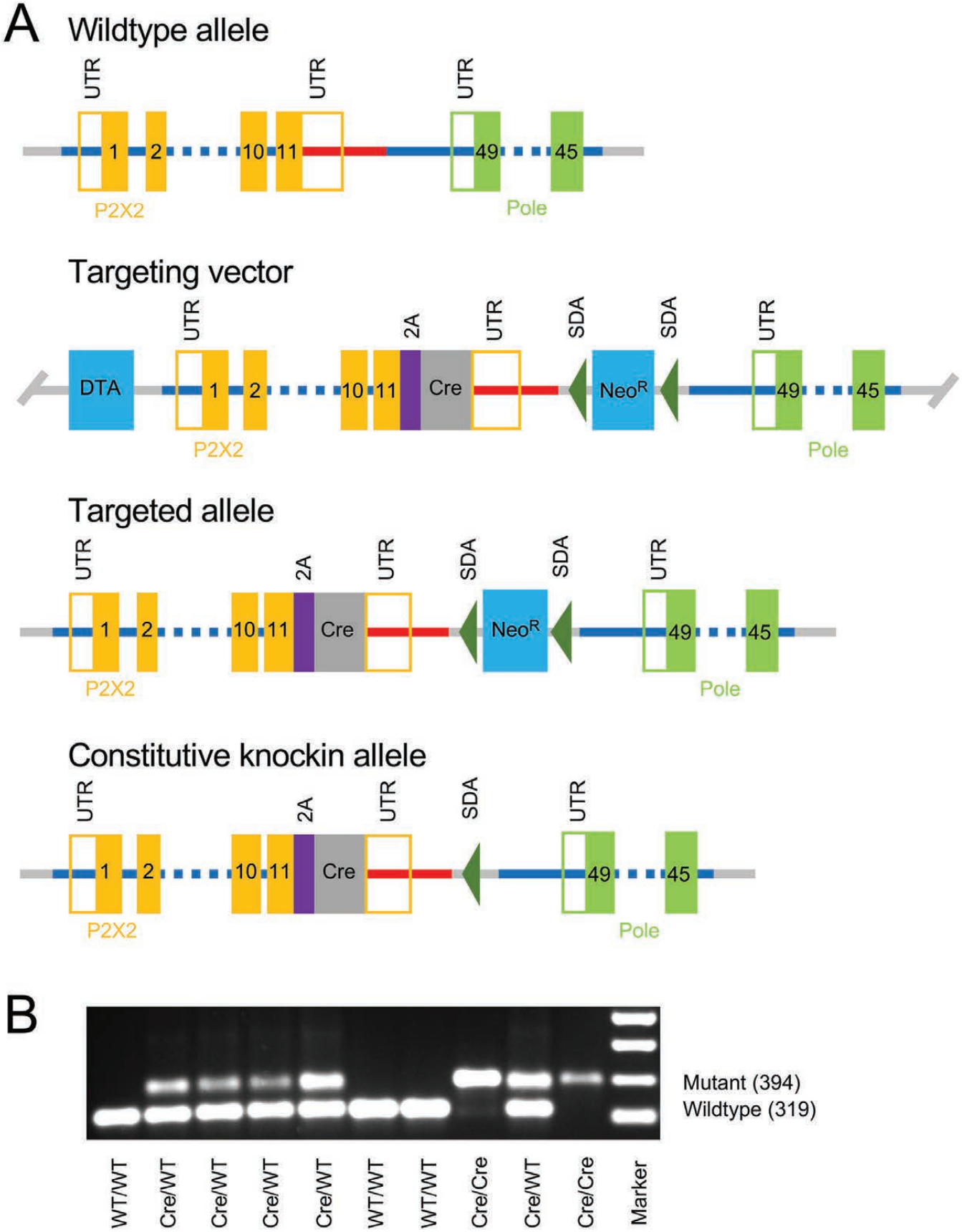

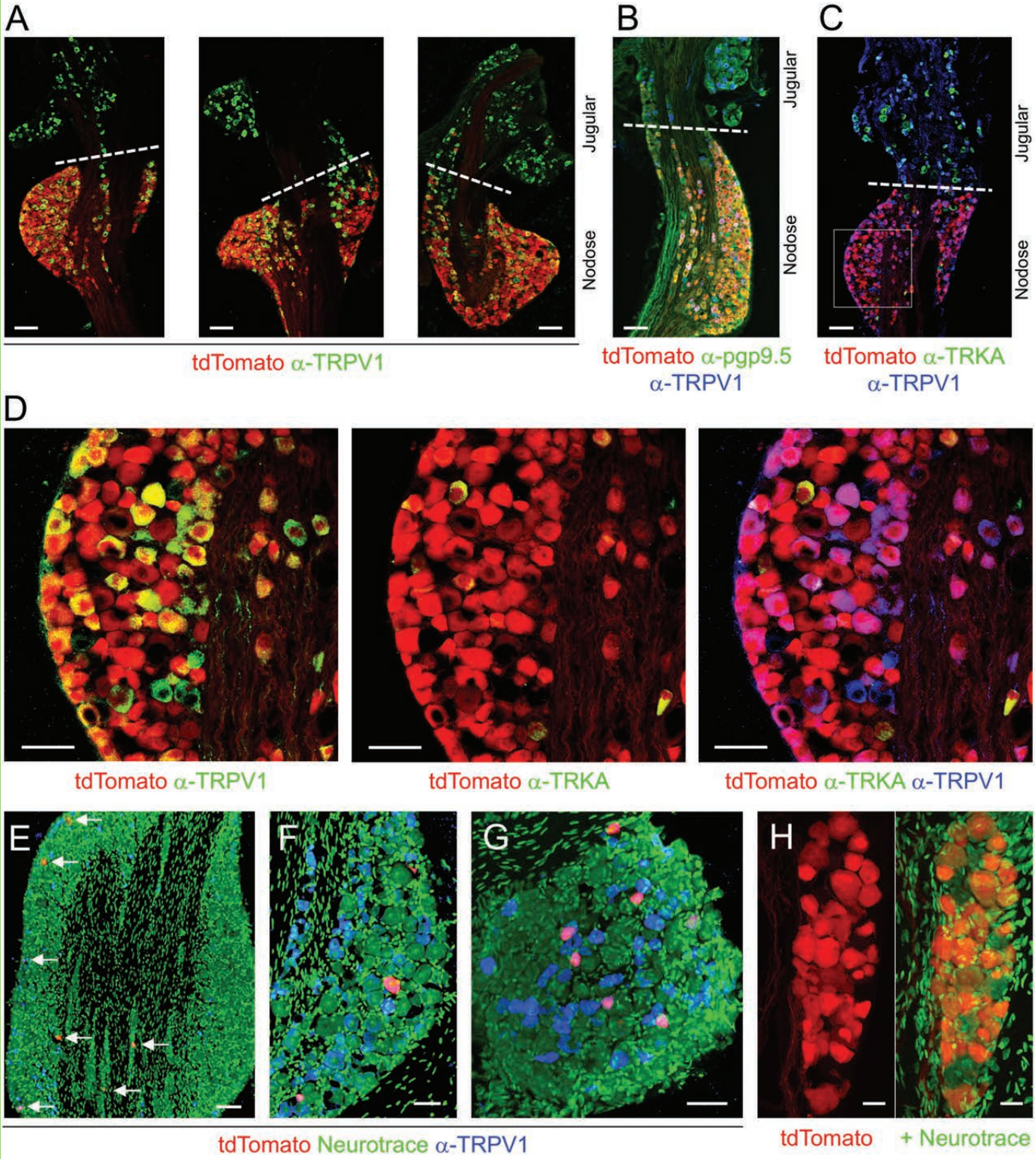

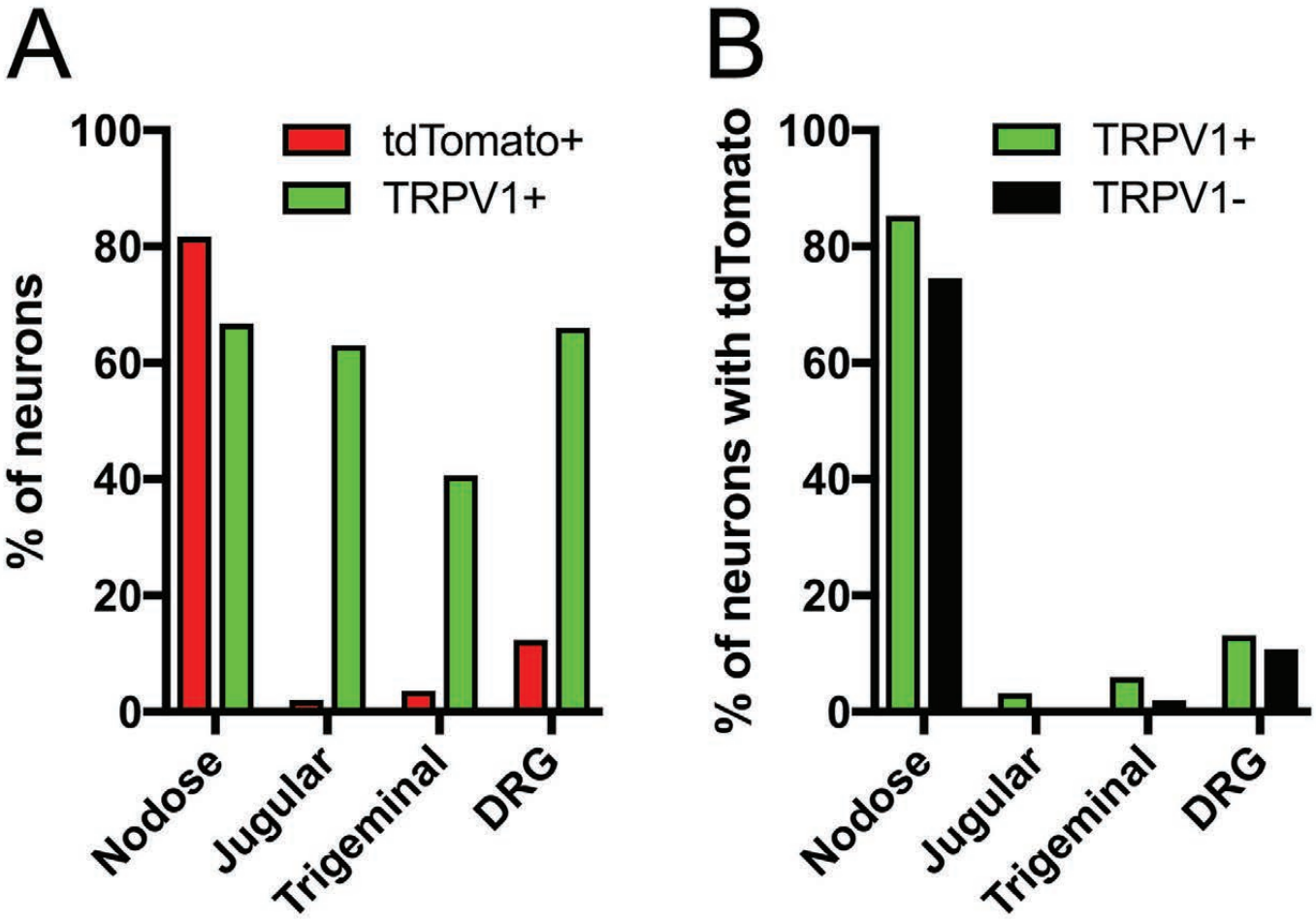

A

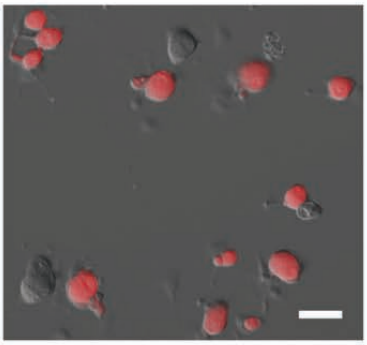

B

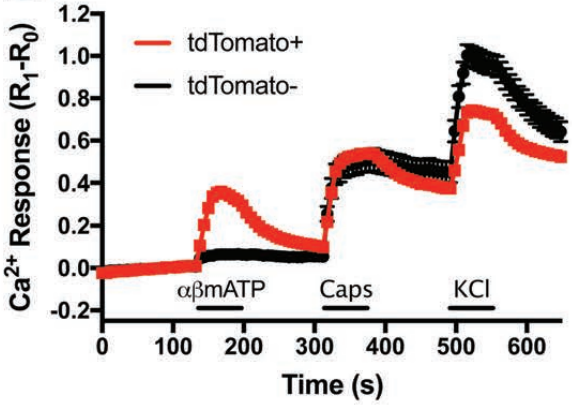

C